

NeRO: Neural Road Surface Reconstruction

Ruibo Wang¹, Song Zhang¹, Ping Huang², Donghai Zhang², and Haoyu Chen²

Z-one Technology Co., LTD. Shanghai, China

{wangruibo01,zhangsong05,huangping01,zhangdonghai,chenhaoyu03}@saicmotor.com

Abstract. In computer vision and graphics, the accurate reconstruction of road surfaces is pivotal for various applications, especially in autonomous driving. This paper introduces a novel method leveraging the Multi-Layer Perceptrons (MLPs) framework to reconstruct road surfaces in height, color, and semantic information by input world coordinates x and y . Our approach **NeRO** uses encoding techniques based on MLPs, significantly improving the performance of the complex details, speeding up the training speed, and reducing neural network size. The effectiveness of this method is demonstrated through its superior performance, which indicates a promising direction for rendering road surfaces with semantics applications, particularly in applications demanding visualization of road conditions, 4D labeling, and semantic groupings.

Keywords: Road Reconstruction · Multi-resolution Hash Positional Encoding · Positional Encoding · Semantic Label

1 Introduction

The evolving landscape of 3D reconstruction has led to significant advancements, especially in reconstructing complex urban environments like road surfaces, which is useful in 4D labeling and semantic groupings. While effective, traditional approaches often grapple with challenges such as computational intensity, low-quality rendering, and semantic information needing improvement.

NeRF presented a method for synthesizing novel views of complex scenes by modeling the volumetric scene function using a fully connected deep neural network. While NeRF’s methodology provides high-quality 3D reconstructions, its application in road surface reconstruction is limited due to its computational requirements. In traditional methods, the result always contains many noisy and incomplete parts. Our work **NeRO** extends this domain by introducing a novel pipeline for road surface reconstruction in different scales, integrating and leveraging semantic information with a small neural network, thus enhancing the reconstruction’s quality and utility.

We use a unified network architecture to reconstruct height, color, and semantics, respectively. And compared different positional encoding methods. For the acquisition of road height information, three methods are used: vehicle camera pose, LiDAR, and SFM. In the future, visual depth estimation can also be used.

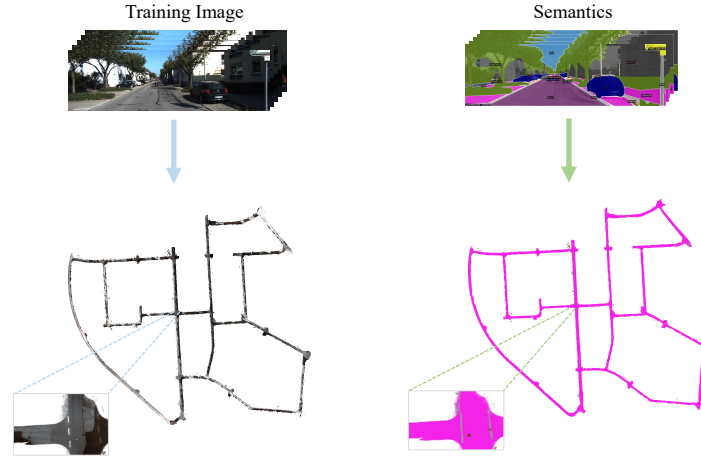


Fig. 1: The result of our method is to reconstruct an entire segment of the road from the KITTI Odometry Sequence 00.

The optimization of the reconstruction process focuses on three critical aspects: the z -coordinate, RGB values, and semantic information. The z -coordinate is derived from various sources mentioned before. Then, we use the output z -value concatenated with the x and y coordinates from the input to the world coordinate for each input. Next, transform each world coordinate into pixel coordinates by extrinsic and intrinsic means to get the actual value from images to compute the loss between RGB outputs and actual RGB values. It also calculates the loss between semantic information outputs and its accurate semantic labels. This optimization process ensures a high-fidelity reconstruction of road surfaces with the semantic context. The main contributions of this paper include:

- We introduce a novel end-to-end MLPs-based road surface reconstruction method, ensuring the quality of road surfaces.
- Our method exhibits semantic abilities when integrating semantic information throughout the reconstruction process.

2 Related Works

Multi-view 2D Image to 3D Reconstruction A notable contribution in this realm is the technique outlined in [20, 21]. Those methods demonstrate a robust capability to reconstruct three-dimensional geometries from two-dimensional images, leveraging known camera poses. In the context of urban mapping, [18] presents a technique that focuses on extracting road line segmentation data from images, followed by an inverse projection of this information to generate three-dimensional maps. Similarly, [26] introduces a method for creating textured meshes from images. [11] explores depth map creation from various viewpoints,

which fuse them into a cohesive three-dimensional structure. [22, 31] capitalizes on the advantages of planar structures, thereby refining the efficiency and accuracy of three-dimensional reconstructions in certain contexts.

NeRF-based Reconstruction Neural Radiance Fields (NeRF) [15] represents an implicit approach, utilizing divergent viewing angles to reconstruct three-dimensional environments. Subsequent research has expanded upon the foundational principles of NeRF, adapting it for extensive, unbounded scenes. Specifically, NeRF++ [33] employs a methodology of normalizing the entirety of a scene into a unit sphere to render the unbounded environments. Further advancements are seen in BlockNeRF [23], which deconstructs large-scale scenes into smaller blocks which processed using the NeRF framework, incorporating elements of exposure and visibility to reconstruct these extensive environments. Conversely, Mip-NeRF 360 [1] introduces an innovative wrapping technique for parameterizing Gaussians, thereby bounding scenes. [10] render the background in single MLPs, and other dynamic objects are learned by a set of MLPs to present a panoptic street view. [3, 12, 19, 30] uses the depth map, LiDAR, and point cloud data to help NeRF give more accurate 3D geometry. In specialized applications, RoME [14] significantly contributes to the reconstruction of road surfaces by optimizing road meshes. MV-Map [29] adopts a voxel-based approach within the NeRF framework like [5, 32], paving the way for the construction of high-definition maps. Moreover, PlaNeRF [27] presents a plane regulation methodology grounded in the decomposition (SVD) technique to reconstruct scenes efficiently with singular values. StreetSurf [8] distinguishes itself by segmenting scenes within images and applying varied scales of multi-resolution hash positional encoding.

NeRF with Semantic There has been much work integrating semantic information into 3D scene reconstruction in the evolving landscape of the implicit method. A pivotal development in this domain is Semantic-NeRF [34], which incorporates an additional layer within the MLPs of NeRF to render the semantic details within three-dimensional environments. Expanding upon this concept, PanopticNeRF [6] merges 3D semantic data with three-dimensional bounding boxes to enhance the geometric fidelity of semantic representations. Another innovative approach is presented in NeRF-SOS [4], which leverages self-supervised learning techniques within the NeRF framework. Furthermore, NeSF (Neural Semantic Fields) [25] demonstrates a unique approach by extracting density information from NeRF outputs, which is processed through a 3D U-Net architecture.

3 Method

We show our framework and pipeline in Fig. 2. **NeRO** processes the input to calculate the height along the vertical z-axis, RGB, and semantic values. In

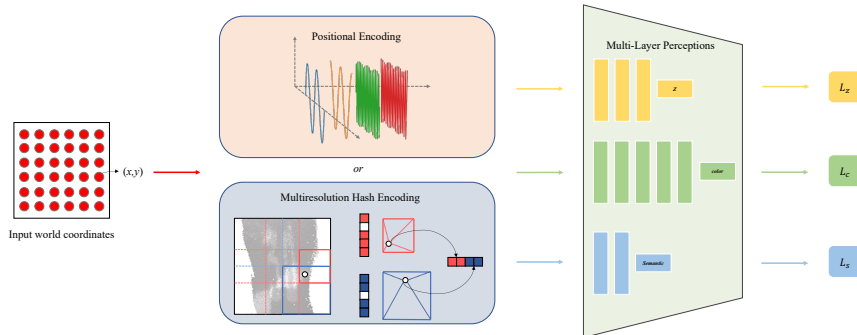


Fig. 2: NeRO Overview. Given the world coordinates $\mathbf{X} = (x, y)$ from the vehicle poses, LiDAR or SfMs are chosen with the Positional Encoding or Multiresolution Positional Encoding to encode the input datasets. Then, the encoded information is passed into three different MLPs responsible for calculating the height z loss, color loss, and semantic loss. The output height z combined with the world coordinates \mathbf{X} will be projected to the image pixels to ensure that color and semantic calculation are only inside the road surface.

Sec. 3.1, we will introduce the overall structure of the network. In Sec. 3.2, we will explain the network integration with encoding methods. In Sec. 3.3, we will illustrate the reconstruction process. In Sec. 3.4, we will describe our training process and loss calculation. These four parts comprise the complete framework, enabling our network to reconstruct road surface information.

3.1 NeRO Network Structure

NeRO takes the x and y coordinates in the world coordinate system, $\mathbf{X} = (x, y)$, as input. Before officially entering the network layers, our input \mathbf{X} is normalized to between $[-1, 1]$ to facilitate the calculation of encoding methods. We feed the normalized input \mathbf{X}' into three different encoding method functions to calculate the vertical z -axis height, RGB, and semantic values. Then, the outputs from the encoding methods are processed by three different MLPs, resulting in outputs for road surface height \mathbf{z} , colour output $\mathbf{c} = (r, g, b)$, and semantic output \mathbf{s} .

3.2 Encoding methods

Positional Encoding From [15, 16, 24], we find that for some high-frequency information, such as color information, direct regression using MLPs fails to capture these high-frequency details. Instead, they tend to learn smoother information. Therefore, to understand these high-frequency details, we need to leverage formulas that utilize Fourier properties to assist MLPs in learning this high-frequency information. In NeRF, Positional Encoding is used to learn high-frequency details with the formula:

$$PE(X) = (\sin(2^0 \pi X), \cos(2^0 \pi X), \dots, \sin(2^{L-1} \pi X), \cos(2^{L-1} \pi X)) \quad (1)$$

Where L is the hyperparameter that decides the length of the function. As demonstrated by various experiments in NeRF, Positional Encoding has significantly aided in achieving excellent rendering results. Our method applies Positional Encoding to the inputs before passing them to the MLPs for subsequent computations.

Multi-Resolution Hash Positional Encoding In [16], a new learnable encoding method, Multi-Resolution Hash Positional Encoding, is introduced. This method first divides the three-dimensional space into 3D grids of various scales. The next step involves obtaining the positions of points within these grids, for which trilinear interpolation is used to determine the specific positional information of the points. These points are then stored in a hash table. Information about these points is retrieved from the hash table during object reconstruction. The retrieved information is transformed into a two-dimensional vector through a learnable embedding layer. Due to overlapping points at different scales, all info is concatenated after embedding before being fed into the MLPs. In our approach, since our network input is a two-dimensional coordinate system, we have established grids at different scales in two dimensions. The specific positional information of points is obtained using bilinear interpolation, and these are also stored in a hash table for subsequent retrieval. We also use a learnable embedding layer to transform these into two-dimensional vectors, concatenate all the information, and then pass it to the MLPs for calculation. Besides that, this method can reduce the network size but still maintain the rendering quality. In our **NeRO**, the network channel is reduced from 256 to 64 by using this method.

3.3 Reconstruction methods

Z-axis Reconstruction We employed ground truth height \mathbf{z}' for supervised learning of network height output \mathbf{z} from three sources: vehicle camera pose, LiDAR datasets, and SfM points. In vehicle camera pose, it is assumed that the ground plane near the corresponding pose is flat, and each pose will sample the points within a length * width certain area in meters. This process optimizes the height network and is used to reconstruct the geometric shape of the road surface. The different representations in the encoding method will affect the result of the height value.

Color Reconstruction In color reconstruction, we sample millions of 2D world coordinates as network input $\mathbf{X} = (x, y)$ for each pose in the first. Then, we use those coordinates to obtain height \mathbf{z} and color \mathbf{c} by height network and color network separately. After that, we combine the road surface height \mathbf{z} with $\mathbf{X} = (x, y)$ to obtain the 3D world coordinates $\mathbf{W} = (x, y, z)$, then transform it into the pixel coordinate system (\mathbf{u}, \mathbf{v}) to get the corresponding ground truth pixel color to optimize network output color \mathbf{c} . Therefore, we need to use the camera’s extrinsic information as the **Tr (Transformation matrix)** and the camera’s intrinsic **K**

information for this calculation. The \mathbf{Tr} includes two parts: the rotation matrix $\mathbf{R} \in \mathbb{R}^{3 \times 3}$, and the translation matrix $\mathbf{t} \in \mathbb{R}^{3 \times 1}$, which represents the camera’s rotation and translation, respectively. The matrix represents the transformation from the camera coordinate system to the world coordinate system. To shift to the pixel coordinate system, we must first transform the world coordinates to the camera coordinate system $\mathbf{C} = (x_c, y_c, z_c)$. We turn the world coordinates into a homogeneous matrix, and then by multiplying it with the inverse of the \mathbf{Tr} , we can obtain the camera coordinates \mathbf{C} . Next, we multiply the intrinsic matrix with the camera coordinates to get the pixel coordinates. The whole formula is as follows:

$$\begin{bmatrix} u \\ v \end{bmatrix} = KC = \begin{bmatrix} f_x & 0 & u_0 \\ 0 & f_y & v_0 \end{bmatrix} \begin{bmatrix} x_c \\ y_c \\ z_c \end{bmatrix} \quad (2)$$

$$= \begin{bmatrix} f_x & 0 & u_0 \\ 0 & f_y & v_0 \end{bmatrix} \begin{bmatrix} R & t \\ 0^T & 1 \end{bmatrix}^{-1} W \quad (3)$$

$$= \begin{bmatrix} f_x & 0 & u_0 \\ 0 & f_y & v_0 \end{bmatrix} \begin{bmatrix} R_{11} & R_{12} & R_{13} & t_x \\ R_{21} & R_{22} & R_{23} & t_y \\ R_{31} & R_{32} & R_{33} & t_z \end{bmatrix}^{-1} \begin{bmatrix} x \\ y \\ z \\ 1 \end{bmatrix} \quad (4)$$

This network color output \mathbf{c} from the encoding methods is used to render the sampled 2D point grids in color, which reconstructs the road surface with the color information.

Semantic Reconstruction The network semantic output \mathbf{s} from the encoding methods is used to render the semantic information for the sampled 2D point grids, which use the same method in color reconstruction to obtain the ground truth semantic \mathbf{s}' . This process reconstructs the road surface with semantics. When adding some noise or reducing the dataset size in training semantic information, that semantic output can still render the road surface with correct semantics.

3.4 Optimization and Loss Function

Our network is divided into three parts: vertical height along the vertical axis \mathbf{z} , color output \mathbf{c} , and semantic output \mathbf{s} . Therefore, we calculate the loss for each of these parts separately.

Z-axis Loss We calculate the loss of Mean Squared Error by the height MLPs F_{Θ}^z output \mathbf{z} with the ground truth \mathbf{z}' , which is the \mathcal{L}_z . We use positional encoding γ or multi-resolution hash positional encoding η to encode the normalized input \mathbf{X}' first and then pass the encoded value to the network to get the height which is $\mathbf{z} = F_{\Theta}^z(\gamma(\mathbf{X}'))$ or $\mathbf{z} = F_{\Theta}^z(\eta(\mathbf{X}'))$.

Color Loss We use the true colour \mathbf{c}' obtained from the pixel coordinate system and compare it with the network output colour \mathbf{c} , which is gained from encoding normalized input by positional encoding γ or multi-resolution hash positional encoding η then passing through the MLPs F_{Θ}^c , the whole process is $\mathbf{c} = F_{\Theta}^c(\gamma(\mathbf{X}'))$ or $\mathbf{c} = F_{\Theta}^c(\eta(\mathbf{X}'))$. After that, it will perform Mean Squared Error loss calculation \mathcal{L}_c . This is done to optimize the RGB layers of the network.

Semantic Loss We use the semantic ground truth \mathbf{s}' and the semantic output \mathbf{s} to perform a Cross-entropy loss calculation \mathcal{L}_s . The semantic output uses either positional encoding γ or multi-resolution hash positional encoding η to encode the normalized input first before proceeding to the MLPs F_{Θ}^s . The process calculates the semantic output is $\mathbf{s} = F_{\Theta}^s(\gamma(\mathbf{X}'))$ or $\mathbf{s} = F_{\Theta}^s(\eta(\mathbf{X}'))$.

Overall Loss The total loss for our method is that:

$$\mathcal{L} = \mathcal{L}_z + \mathcal{L}_c + \mathcal{L}_s \quad (5)$$

$$= \sum_{n=1}^N \left[\|z - z'\|_2^2 + \|c - c'\|_2^2 + \sum_{l=1}^L s \log(s') \right] \quad (6)$$

Where N is the number of points inside the road surface that appear in the road part of the training images, and L is the number of semantic labels used in the training process.

4 Experiment

4.1 Experiment Settings

Datasets Our experiment uses Kitti [7] datasets to test our method. The Kitti odometry datasets contain 22 sequences, which use the first 11 sequences (00 - 10) as the training sequence and the last 11 sequences (11 - 21) as the test sequence. In our experiment, we use the data from sequence 00. In sequence 00, there are 4541 images, and in our experiment, we use all images from the left camera as our training datasets to obtain the extrinsic information, LiDAR datasets and the camera height in vehicle pose. The Kitti odometry datasets do not have any semantic information. We use the state-of-the-art semantic prediction method Mask2Former [2] to acquire that information. In the Mask2Former, we chose the Swin-L [13] backbone to predict the semantic label. After obtaining the semantic labels, we use those labels to eliminate the objects that do not appear on the road to our training images and semantic datasets. The SfM datasets are obtained by COLMAP, which uses the camera pose and RGB image information from those images to create sparse or dense points cloud.

Evaluation Metrics As our experiment compares the pixel color from the ground images, the metric for that is using PSNR to verify the quality of our rendering ability. Our method also needs to compare the semantic label accuracy so that the metric to reach that is mIoU.

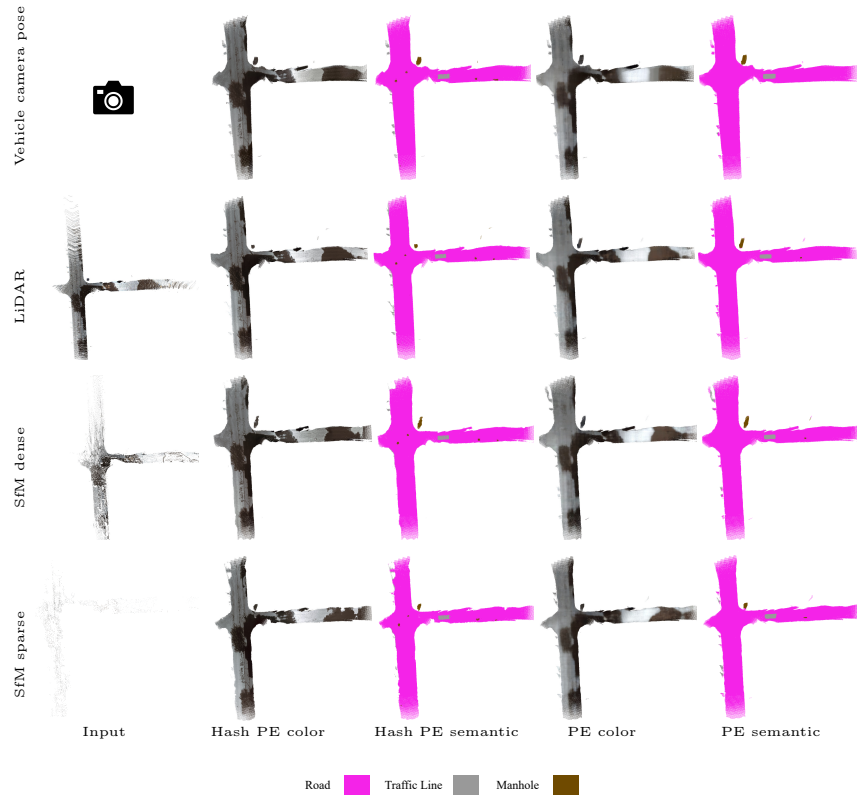


Fig. 3: In qualitative comparison with the PE and Hash PE in the datasets of the vehicle camera pose, LiDAR points, SfMs dense points, and SfMs sparse points. The first column shows each input dataset, and the rest illustrates the reconstruction result. Hash PE has a better render quality in each result than in color and semantics.

Setup Environment The PyTorch implements the method Pytorch [17] framework, which uses the Nvidia A100 80G to train our model. The training images are the original fixed size, 1241 x 376, with batch size 1. The training optimizer we selected is Adam [9], with a learning rate of 5e-4.

4.2 Reconstruct Incomplete Road Surfaces With Different Height

To illustrate the effectiveness of the encoding methods representation, an experimental setup was utilized featuring a square wave-like road structure, incorporating two distinct holes located on the horizontal and the corner of the plane in the road surface, as depicted in the Fig. 4. The positional encoding method successfully fills these holes, accurately replicating the correct shape. This effectiveness is attributed to its inherent periodic property, which provides prior information. However, a limitation of this approach is the lack of smoothness on the road

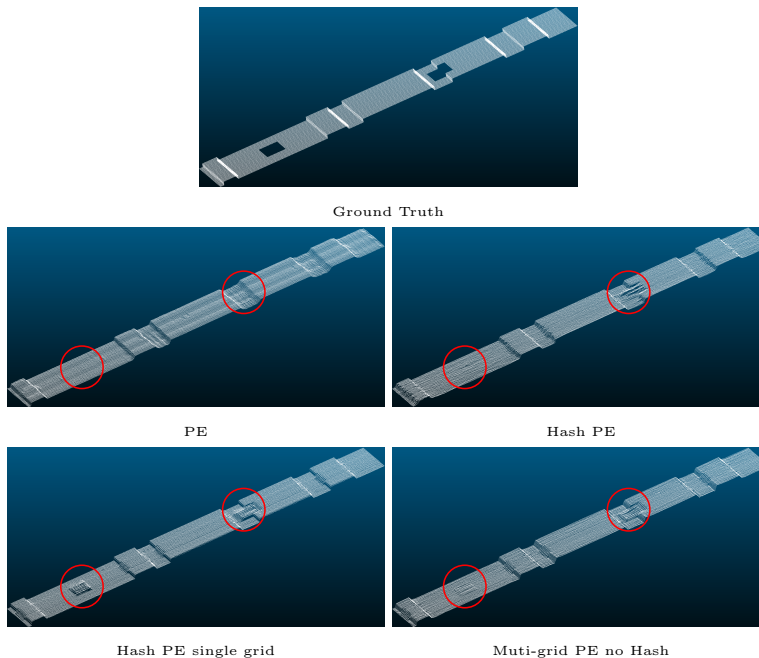


Fig. 4: Comparison in reconstructing the incomplete road. The first row shows the ground truth dataset with two holes. In the second row, the left side shows the positional encoding result and the right side shows the multi-resolution positional encoding result. In the last row, the left side is the result of only using one grid with the hash function, and the right side illustrates the result of using multiple grids without the hash function. The red circle indicates the hole in the horizontal and corner of the road surface.

surface. Multi-resolution hash positional encoding excels in rendering the road surface with remarkable smoothness. It fills the horizontal holes smoothly and attempts to fill the corner holes with values from adjacent areas. This is due to the absence of prior information in the multi-resolution hash positional encoding approach, leading to a less smooth appearance. We also examine the ability of multi-resolution hash positional encoding when it has only a single resolution or devoid hash function. The figure shows that only a single hash function without multiresolution cannot fill horizontal and corner holes. Conversely, employing a multiresolution approach without a hash function demonstrates a filling capability similar to the multi-resolution hash positional encoding method. But look in detail, it still has some marks of filling.

4.3 Color And Semantic Result In Different PE methods

In this part, we show our experiment results in color and semantic results in different positional encoding methods for our method **NeRO** with different input datasets, and in Tab. 1, we offer our quantitative metric for each result.

Table 1: Quantitive result for our method in reconstructing the road surface in color and semantics with the dataset from vehicle camera pose, LiDAR, and SfMs using multi-resolution hash positional encoding or positional encoding method.

Datasets	Positional Encoding Type	PSNR	mIoU
Vehicle Camera Pose	PE	17.81	0.704
Vehicle Camera Pose	Hash PE	25.73	0.988
LiDAR	PE	18.87	0.701
LiDAR	Hash PE	29.20	0.994
SfM-Dense	PE	18.76	0.784
SfM-Dense	Hash PE	25.81	0.975
SfM-Sparse	PE	18.38	0.780
SfM-Sparse	Hash PE	24.37	0.967

Vehicle Camera Pose The methodology involves the utilization of either positional encoding or multi-resolution hash positional encoding. The comparison of these two approaches is visually evident in the results presented in the Fig. 3. Within the positional encoding framework, while the road structure is discernibly captured, the detail of the road surface, like the speed limit warning line and road texture, needs to be clearer. Conversely, multi-resolution hash positional encoding not only distinctly displays the speed limit warning line but also enhances the textural representation of the road surface. When focusing on the semantic results, both positional encoding and multi-resolution hash positional encoding effectively reconstruct the structural components of the road surface, including aspects of the speed limit warning line. However, in smaller parts such as manholes, only the multi-resolution hash positional encoding method can accurately learn and represent these elements.

LiDAR Points The Fig. 3 illustrates that positional encoding and multi-resolution hash positional encoding methods are applied to the LiDAR point clouds. These methods enable the supplementation of these clouds with learned 3D points, thereby approximating the original structure. The comparison result is similar to the previous one: only the multi-resolution hash positional encoding method successfully renders both the speed limit warning lines with high fidelity. A notable difference is represented when examining the semantic results of the two methods. The multi-resolution hash positional encoding method successfully identifies and renders all manholes on the road surface. On the other hand, the positional encoding method exhibits limitations, identifying and rendering only a single manhole cover.

SfM Points The **Dense** point clouds section, characterised by a higher concentration of points, shows that positional encoding and multi-resolution hash positional encoding methods are applied to the dense part. The results are consistent with previous observations, and only multi-resolution hash positional encoding

Table 2: Quantitive result for our method for sparse labels. When using only 10% training semantic dataset, the positional encoding or multi-resolution hash positional encoding method is processed to reconstruct the road surface in LiDAR datasets.

Sparse Ratio	Positional Encoding Type	mIoU
0.1	PE	0.670
0.1	Hash PE	0.823

Table 3: The quantitive result for our method is denoising the noisy semantic labels, which use positional encoding or multi-resolution hash positional encoding method to denoise the label with the noise ratio when 50% or 90% labels are noised in LiDAR datasets.

Noise Ratio	Positional Encoding Type	mIoU
0.5	PE	0.693
0.5	Hash PE	0.625
0.9	PE	0.420
0.9	Hash PE	0.292

renders the entire road surface with remarkable detail and accuracy. The positional encoding and multi-resolution hash positional encoding methods are again assessed when examining the **Sparse** point clouds section, noted for its fewer points. The outcomes here mirror those observed in the dense cloud context. An observation in dense and sparse scenarios is that road sections lack point data. However, regardless of the point cloud density, our method can fill those hollows with appropriate color and structure. The result is shown in Fig. 3.

4.4 Semantic Labels Applications

This section shows how our method is applied in some applications, like sparse labels and semantic label denoising. In NeRF-based models, like [28, 34] offer its ability on that kind of application. We only chose the LiDAR dataset for this process because it has relatively accurate road height values. And in Tab. 2 and Tab. 3, we offer our quantitive metric for each result.

Sparse Label We hypothesise a scenario where a significant portion of ground truth semantic images is unavailable, leaving only a minimal subset for use. From [34], it indicated that using less than 10% of semantic images will significantly decrease the rendering quality. Our investigation will set the threshold to only 10% of images to evaluate whether our method could reconstruct the road surface. Fig. 5 presents the outcomes by using positional encoding or multi-resolution hash positional encoding. The results demonstrate that, despite the limited availability of training semantics, both methods can reconstruct the

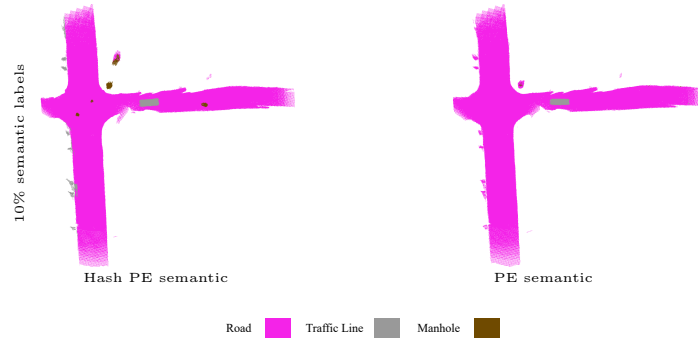


Fig. 5: Qualitative comparison with the positional encoding and multi-resolution hash positional encoding in the sparse semantic labels. Both methods render the whole structure of the road, but the Hash PE on the left gives more detail in the result.

road surfaces. However, the distinct advantage of multi-resolution hash positional encoding is its ability to render detailed features, such as manholes, which positional encoding fails to replicate with the same level of detail. Tab. 2 shows the quantitative result in the mIoU. Here, it is evident that multi-resolution hash positional encoding outperforms positional encoding, showcasing superior mIoU values.

Denoise Label In the actual scenarios, the road datasets have noise content, so we add some pixel noises to the ground truth, and the noised semantic labels are used to examine our method’s denoise ability. Fig. 6 illustrates the outcomes of applying denoising reconstruction to noisy labels using positional encoding or multi-resolution hash positional encoding. In scenarios with 50% noise in the labels, it is observed that both multi-resolution hash positional encoding and positional encoding can reconstruct the road surface, but the positional encoding method fails to reconstruct some specific items, like manholes in the middle of the road. When we add the ratio of noise labels to 90%, multi-resolution hash positional encoding cannot denoise the label due to its accurate learning ability. Its precision in learning leads to the unintentional incorporation of noise labels as road surface components. In contrast, the positional encoding method continues to denoise the labels. However, it can still not render detailed features like manholes in the middle of the road. The quantitative analysis in Tab. 3 shows that the mIoU value of positional encoding is higher than multi-resolution hash positional encoding, indicating a better semantic denoise ability. Still, positional encoding needs to be more comprehensive in rendering the details. Further investigations were conducted to determine the noise ratio threshold of the denoise ability of multi-resolution hash positional encoding. Visual results indicate that multi-resolution hash positional encoding begins to integrate noise labels into the road surface when the noise ratio exceeds 0.6.



Fig. 6: Qualitative comparison with the positional encoding and multi-resolution hash positional encoding in the noisy semantic labels. The first column shows the input noisy datasets, the second column records the multi-resolution hash positional encoding result, and the final column gives the positional encoding result.

4.5 Training speed

During the networks’ training phase, the loss reduction is shown in the Fig. 7. When examining the vertical z-axis loss, both positional encoding and multi-resolution hash positional encoding methods exhibit comparable training speeds, ultimately converging on their global minima. Multi-resolution hash positional encoding demonstrates an accelerated color and semantic loss training speed, efficiently attaining the global minima. Conversely, the positional encoding method experiences a slower decrease in loss, facing challenges in achieving convergence to the global minima.

5 Limitation

The limitation of our method is the difficulty in achieving a balance between noise reduction and the delineation of raised and flat segments on road surfaces. We encounter some problems in calibrating positional encoding or multi-resolution hash positional encoding. Specifically, when the parameter value is minimized, the methodology tends to amalgamate raised and flat sections, resulting in a road surface that exhibits a wave-like appearance. This outcome diverges from

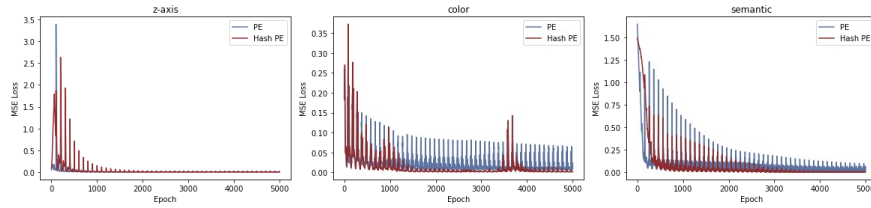


Fig. 7: Comparison in the training loss decay between positional encoding and multi-resolution hash positional encoding in the z-axis, color, and semantic.

the original road surfaces, wherein the horizontal sections maintain a distinct angular relationship to those convex parts. Setting a higher parameter value yields a road surface that more closely resembles the original road surfaces. However, this adjustment introduces some noise appearing on the road surface. In future research, we propose to refine our approach by incorporating a smaller network to learn the vertical height of the road surface. Additionally, we aim to employ an occupancy network to reconstruct raised road sections, thereby addressing the current limitations and improving the overall quality of our model.

6 Conclusion

In conclusion, we illustrate an end-to-end MLPs-based neural road reconstruction method that accepts the various sources of datasets to render the color and semantic information with road height output. Our experiment shows the success of our rendering ability in either color or semantic information. In the semantic applications, it also shows that it can handle sparse labels and noise labels. We also compare the Positional Encoding and Multi-resolution Positional Encoding methods to deliver each performance. This indicates that the Multi-resolution Positional Encoding method performs better in rendering the road surfaces in quality and speed.

References

1. Barron, J.T., Mildenhall, B., Verbin, D., Srinivasan, P.P., Hedman, P.: Mip-nerf 360: Unbounded anti-aliased neural radiance fields. In: Proceedings of the IEEE/CVF Conference on Computer Vision and Pattern Recognition. pp. 5470–5479 (2022) [3](#)
2. Cheng, B., Misra, I., Schwing, A.G., Kirillov, A., Girdhar, R.: Masked-attention mask transformer for universal image segmentation. In: Proceedings of the IEEE/CVF conference on computer vision and pattern recognition. pp. 1290–1299 (2022) [7](#)
3. Deng, K., Liu, A., Zhu, J.Y., Ramanan, D.: Depth-supervised nerf: Fewer views and faster training for free. In: Proceedings of the IEEE/CVF Conference on Computer Vision and Pattern Recognition. pp. 12882–12891 (2022) [3](#)
4. Fan, Z., Wang, P., Jiang, Y., Gong, X., Xu, D., Wang, Z.: Nerf-sos: Any-view self-supervised object segmentation on complex scenes. arXiv preprint arXiv:2209.08776 (2022) [3](#)
5. Fridovich-Keil, S., Yu, A., Tancik, M., Chen, Q., Recht, B., Kanazawa, A.: Plenoxels: Radiance fields without neural networks. In: Proceedings of the IEEE/CVF Conference on Computer Vision and Pattern Recognition. pp. 5501–5510 (2022) [3](#)
6. Fu, X., Zhang, S., Chen, T., Lu, Y., Zhu, L., Zhou, X., Geiger, A., Liao, Y.: Panoptic nerf: 3d-to-2d label transfer for panoptic urban scene segmentation. In: 2022 International Conference on 3D Vision (3DV). pp. 1–11. IEEE (2022) [3](#)
7. Geiger, A., Lenz, P., Urtasun, R.: Are we ready for autonomous driving? the kitti vision benchmark suite. In: 2012 IEEE conference on computer vision and pattern recognition. pp. 3354–3361. IEEE (2012) [7](#)
8. Guo, J., Deng, N., Li, X., Bai, Y., Shi, B., Wang, C., Ding, C., Wang, D., Li, Y.: Streetsurf: Extending multi-view implicit surface reconstruction to street views. arXiv preprint arXiv:2306.04988 (2023) [3](#)
9. Kingma, D.P., Ba, J.: Adam: A method for stochastic optimization. arXiv preprint arXiv:1412.6980 (2014) [8](#)
10. Kundu, A., Genova, K., Yin, X., Fathi, A., Pantofaru, C., Guibas, L.J., Tagliasacchi, A., Dellaert, F., Funkhouser, T.: Panoptic neural fields: A semantic object-aware neural scene representation. In: Proceedings of the IEEE/CVF Conference on Computer Vision and Pattern Recognition. pp. 12871–12881 (2022) [3](#)
11. Leroy, V., Franco, J.S., Boyer, E.: Shape reconstruction using volume sweeping and learned photoconsistency. In: Proceedings of the European Conference on Computer Vision (ECCV). pp. 781–796 (2018) [2](#)
12. Li, Z., Li, L., Ma, Z., Zhang, P., Chen, J., Zhu, J.: Read: Large-scale neural scene rendering for autonomous driving. arxiv preprint [2022-12-11] (2022) [3](#)
13. Liu, Z., Lin, Y., Cao, Y., Hu, H., Wei, Y., Zhang, Z., Lin, S., Guo, B.: Swin transformer: Hierarchical vision transformer using shifted windows. In: Proceedings of the IEEE/CVF international conference on computer vision. pp. 10012–10022 (2021) [7](#)
14. Mei, R., Sui, W., Zhang, J., Zhang, Q., Peng, T., Yang, C.: Rome: Towards large scale road surface reconstruction via mesh representation. arXiv preprint arXiv:2306.11368 (2023) [3](#)
15. Mildenhall, B., Srinivasan, P.P., Tancik, M., Barron, J.T., Ramamoorthi, R., Ng, R.: Nerf: Representing scenes as neural radiance fields for view synthesis. Communications of the ACM **65**(1), 99–106 (2021) [3](#), [4](#)

16. Müller, T., Evans, A., Schied, C., Keller, A.: Instant neural graphics primitives with a multiresolution hash encoding. *ACM Transactions on Graphics (ToG)* **41**(4), 1–15 (2022) [4](#), [5](#)
17. Paszke, A., Gross, S., Massa, F., Lerer, A., Bradbury, J., Chanan, G., Killeen, T., Lin, Z., Gimelshein, N., Antiga, L., et al.: Pytorch: An imperative style, high-performance deep learning library. *Advances in neural information processing systems* **32** (2019) [8](#)
18. Qin, T., Zheng, Y., Chen, T., Chen, Y., Su, Q.: A light-weight semantic map for visual localization towards autonomous driving. In: 2021 IEEE International Conference on Robotics and Automation (ICRA). pp. 11248–11254. IEEE (2021) [2](#)
19. Rematas, K., Liu, A., Srinivasan, P.P., Barron, J.T., Tagliasacchi, A., Funkhouser, T., Ferrari, V.: Urban radiance fields. In: Proceedings of the IEEE/CVF Conference on Computer Vision and Pattern Recognition. pp. 12932–12942 (2022) [3](#)
20. Schonberger, J.L., Frahm, J.M.: Structure-from-motion revisited. In: Proceedings of the IEEE conference on computer vision and pattern recognition. pp. 4104–4113 (2016) [2](#)
21. Schönberger, J.L., Zheng, E., Frahm, J.M., Pollefeys, M.: Pixelwise view selection for unstructured multi-view stereo. In: Computer Vision–ECCV 2016: 14th European Conference, Amsterdam, The Netherlands, October 11–14, 2016, Proceedings, Part III 14. pp. 501–518. Springer (2016) [2](#)
22. Sun, S., Zheng, Y., Shi, X., Xu, Z., Liu, Y.: Phi-mvs: Plane hypothesis inference multi-view stereo for large-scale scene reconstruction. *arXiv preprint arXiv:2104.06165* (2021) [3](#)
23. Tancik, M., Casser, V., Yan, X., Pradhan, S., Mildenhall, B., Srinivasan, P.P., Barron, J.T., Kretzschmar, H.: Block-nerf: Scalable large scene neural view synthesis. In: Proceedings of the IEEE/CVF Conference on Computer Vision and Pattern Recognition. pp. 8248–8258 (2022) [3](#)
24. Tancik, M., Srinivasan, P., Mildenhall, B., Fridovich-Keil, S., Raghavan, N., Singhal, U., Ramamoorthi, R., Barron, J., Ng, R.: Fourier features let networks learn high frequency functions in low dimensional domains. *Advances in Neural Information Processing Systems* **33**, 7537–7547 (2020) [4](#)
25. Vora, S., Radwan, N., Greff, K., Meyer, H., Genova, K., Sajjadi, M.S., Pot, E., Tagliasacchi, A., Duckworth, D.: Nsf: Neural semantic fields for generalizable semantic segmentation of 3d scenes. *arXiv preprint arXiv:2111.13260* (2021) [3](#)
26. Waechter, M., Moehrle, N., Goesele, M.: Let there be color! large-scale texturing of 3d reconstructions. In: Computer Vision–ECCV 2014: 13th European Conference, Zurich, Switzerland, September 6–12, 2014, Proceedings, Part V 13. pp. 836–850. Springer (2014) [2](#)
27. Wang, F., Louys, A., Piasco, N., Bennehar, M., Roldão, L., Tsishkou, D.: Planerf: Svd unsupervised 3d plane regularization for nerf large-scale scene reconstruction. *arXiv preprint arXiv:2305.16914* (2023) [3](#)
28. Wang, R., Zhang, S., Huang, P., Zhang, D., Yan, W.: Semantic is enough: Only semantic information for nerf reconstruction. In: 2023 IEEE International Conference on Unmanned Systems (ICUS). pp. 906–912. IEEE (2023) [11](#)
29. Xie, Z., Pang, Z., Wang, Y.X.: Mv-map: Offboard hd-map generation with multi-view consistency. In: Proceedings of the IEEE/CVF International Conference on Computer Vision. pp. 8658–8668 (2023) [3](#)
30. Xu, Q., Xu, Z., Philip, J., Bi, S., Shu, Z., Sunkavalli, K., Neumann, U.: Point-nerf: Point-based neural radiance fields. In: Proceedings of the IEEE/CVF Conference on Computer Vision and Pattern Recognition. pp. 5438–5448 (2022) [3](#)

31. Xu, Q., Tao, W.: Planar prior assisted patchmatch multi-view stereo. In: Proceedings of the AAAI Conference on Artificial Intelligence. vol. 34, pp. 12516–12523 (2020) [3](#)
32. Yu, A., Li, R., Tancik, M., Li, H., Ng, R., Kanazawa, A.: Plenotrees for real-time rendering of neural radiance fields. In: Proceedings of the IEEE/CVF International Conference on Computer Vision. pp. 5752–5761 (2021) [3](#)
33. Zhang, K., Riegler, G., Snavely, N., Koltun, V.: Nerf++: Analyzing and improving neural radiance fields. arXiv preprint arXiv:2010.07492 (2020) [3](#)
34. Zhi, S., Laidlow, T., Leutenegger, S., Davison, A.J.: In-place scene labelling and understanding with implicit scene representation. In: Proceedings of the IEEE/CVF International Conference on Computer Vision. pp. 15838–15847 (2021) [3](#), [11](#)